Agonist-Induced Changes in Ca^{2+} Permeation through the Nociceptor Cation Channel TRPA1

Yuji Karashima, Jean Prenen, Karel Talavera, Annelies Janssens, Thomas Voets,* and Bernd Nilius
Department of Molecular Cell Biology, Laboratory of Ion Channel Research, Katholieke Universiteit Leuven, Leuven, Belgium

ABSTRACT The Ca^{2+}-permeable cation channel TRPA1 acts as an ionotropic receptor for various pungent compounds and as a noxious cold sensor in sensory neurons. It is unclear what proportion of the TRPA1-mediated current is carried by Ca^{2+} ions and how the permeation pathway changes during stimulation. Here, based on the relative permeability of the nonstimulated channel to cations of different size, we estimated a pore diameter of ~11 Å. Combined patch-clamp and Fura-2 fluorescence recordings revealed that with 2 mM extracellular Ca^{2+}, and at a membrane potential of −80 mV, ~17% of the inward TRPA1 current is carried by Ca^{2+}. Stimulation with mustard oil evoked an apparent dilatation of the pore of 3 Å and an increase in divalent cation selectivity and fractional Ca^{2+} current. Mutations in the putative pore that reduced the divalent permeability and fractional Ca^{2+} current also prevented mustard-oil-induced increases in Ca^{2+} permeation. It is interesting that fractional Ca^{2+} currents for wild-type and mutant TRPA1 were consistently higher than values predicted based on biionic reversal potentials using the Goldman-Hodgkin-Katz equation, suggesting that binding of Ca^{2+} in the pore hinders monovalent cation permeation. We conclude that the pore of TRPA1 is dynamic and supports a surprisingly large Ca^{2+} influx.

INTRODUCTION

The nonselective cation channel TRPA1 is highly expressed in a subpopulation of primary afferent sensory nociceptive neurons, where its activation causes pain (1–4). TRPA1 can be gated by various stimuli, including noxious cold (1,5), intracellular Ca^{2+} and Zn^{2+} ions (6–8), intracellular alkalinization (9), and a plethora of pungent and/or noxious chemical compounds (10–12). Many of the TRPA1 agonists, including isothiocyanates such as mustard oil and reactive aldehydes such as cinnamaldehyde or acrolein, are thiol-reactive electrophiles that activate TRPA1 through a covalent binding with cysteine and lysine residues in the cytosolic part of the channel (13,14). Other, nonelectrophile agonists of the channel include icilin, THC, menthol and menthol-analogs, clotrimazole, dihydropyridines, nicotine, and general anesthetics such as propofol (1,11,15).

In contrast with the overwhelming information on TRPA1 activators/modulators (16–19), relatively few reports have addressed the biophysical properties of the TRPA1 pore. It has been recently shown that Ca^{2+} selectivity is affected by mutations of a conserved aspartate residue (Asp^{918}) in the putative selectivity filter (20). Yet, it is unclear how much of the inward TRPA1 current is actually carried by Ca^{2+}, or whether this Ca^{2+} permeability can be dynamically modulated. Reports on the permeability of Ca^{2+} (P_{Ca}) relative to that of monovalent cations as determined from reversal-potential measurements are inconsistent, yielding values for P_{Ca}/P_{Na} ranging from 0.84 (1) to 3.3 (20). Accurate determination of the amount of Ca^{2+} entering via the TRPA1 pore is particularly important for several reasons. First of all, Ca^{2+} entry through the TRPA1 pore can heavily modulate TRPA1 activation and subsequent desensitization during agonist-induced stimulation (6,7,20,21). Moreover, Ca^{2+} entry into nociceptor neurons can modulate the activity of other channels and induce the release of neurogenic peptides such as substance P. In addition to the entry of Ca^{2+}, TRPA1 may also mediate passage of larger cations, but the dimensions of the TRPA1 permeation pathway are currently unknown.

Here, we present a systematic study of the pore of TRPA1, including a determination of the apparent diameter of the pore and of the contribution of Ca^{2+} to the inward TRPA1 current. Our results reveal a wide pore of at least 11 Å in diameter and indicate that Ca^{2+} contributes to a larger extent to the inward current than would be expected based on reversal-potential measurements. Moreover, we present evidence for a dynamic regulation of the pore during agonist stimulation, leading to an apparent dilatation of the pore, an increased divalent permeability, and a larger fractional Ca^{2+} current.

MATERIALS AND METHODS

Cell culture

Tetracycline-inducible Chinese hamster ovary (CHO) cells stably expressing mouse TRPA1 (kindly provided by Dr. A. Patapoutian, Scripps Research Institute, La Jolla, CA) were grown in Dulbecco's modified Eagle's medium containing 10% (v/v) human serum, 1% (v/v) nonessential amino acids, 2 mM L-glutamine, 2 units/ml penicillin, 2 mg/ml streptomycin, 100 μg/ml hygromycin B, and 5 g/ml blasticidin at 37°C in a humidity-controlled incubator with 5% CO_2. To induce expression of TRPA1, 0.5 μg/ml tetracycline was added to the culture medium, and cells were used 3–12 h after induction. In an alternative preparation, regular CHO cells were grown in Ham's F12 medium containing 10% (v/v) human serum, 2 mM L-glutamine, 2 units/ml penicillin, and 2 mg/ml streptomycin at 37°C in a humidity-controlled

Submitted August 25, 2009, and accepted for publication November 5, 2009.

*Correspondence: thomas.voets@med.kuleuven.be

Editor: Marc Baldus.

0006-3495/10/03/0773/11 $2.00

doi: 10.1016/j.bpj.2009.11.007

incubator with 5% CO_2 and then transiently transfected with wild-type (WT) or mutant mouse TRPA1 cloned in the bicistronic pCAGGS-IRES-GFP vector using TransIT-293 transfection reagent (Mirus, Gøteborg, Sweden). Transfected cells were identified by their green fluorescence and used between 16 and 24 h after transfection.

Solutions and drugs

Extracellular solutions were applied via a gravity-driven perfusion system whose outlet was placed within 500 μm of the cells under investigation; full solution exchange was achieved within 2 s.

To study the relative permeability of monovalent cations we used extracellular solutions containing (in mM) 10 glucose, 10 HEPES, and 150 XCl, where X^+ represents the monovalent cation. These solutions were titrated to pH 7.4 with the appropriate base (XOH). To measure the relative permeability of Ca^{2+} or Mg^{2+} extracellular solutions containing 10 glucose, 10 HEPES, and 100 $CaCl_2$ or $MgCl_2$ (pH 7.4 with $Ca(OH)_2$ or $Mg(OH)_2$) were used. The pipette solution for these experiments contained (in mM) 150 NaCl, 5 ethylene-glycol-O,O′-bis(2-aminoethyl)-N,N,N′,N′-tetraacetic acid (EGTA), and 10 HEPES, pH 7.2 with NaOH.

For the fractional Ca^{2+} current experiments, the intracellular solution contained (in mM) 150 NaCl, 1 $MgCl_2$, 10 HEPES, and 5 K_5Fura-2, pH 7.2 with NaOH. All of the extracellular solutions in these experiments contained 1 $MgCl_2$, 10 glucose, and 10 HEPES, with an added 150 NaCl and 1 EGTA for the Ca^{2+}-free solutions, 150 NaCl and 2 $CaCl_2$ for the 2-Ca^{2+} solution, and 100 $CaCl_2$ for the isotonic Ca^{2+} solution.

The pipette solutions used for cell-attached and inside-out recordings contained (in mM) 1 or 5 $MgCl_2$, 150 NaCl, and 10 HEPES, pH 7.4. For the cell-attached recordings, the bath solution contained 150 CsCl, 1 $MgCl_2$, 3 $CaCl_2$, 5 EGTA, and 10 HEPES, pH 7.2 with CsOH. The estimated free-Ca^{2+} concentration of this solution is 250 nM. For inside-out recordings, this bath solution was supplemented with 2 MgATP to prevent run-down.

The extracellular solution used in ratiometric $[Ca^{2+}]_i$ measurements contained (in mM) 140 NaCl, 5 KCl, 1 $MgCl_2$, 5 glucose, and 10 HEPES, supplemented with either 2 $CaCl_2$ or 1 mM EGTA and titrated to pH 7.4. The extracellular solution used in FM1-43 uptake experiments contained (in mM) 140 NaCl, 5 KCl, 1 $MgCl_2$, 5 glucose, and 10 HEPES, pH 7.4.

Mustard oil (MO; allyl isothiocyanate) and ruthenium red were purchased from Sigma (St. Louis, MO), HC030031 from Tocris (Bristol, United Kingdom), K_5Fura-2 from TEF Labs (Austin, TX), and FM1-43 (SynaptoGreen C4) from Biotium (Hayward, CA). Experiments were performed at room temperature (22–25°C).

Electrophysiology

Whole-cell currents and single-channel currents were measured using EPC-7 or EPC-9 patch-clamp amplifiers (HEKA Elektronik, Lambrecht, Germany). Patch electrodes had a DC resistance between 2 and 4 MΩ when filled with the different recording solutions. In whole-cell recordings, between 50 and 80% of the series resistance was electronically compensated to minimize voltage errors, and currents were sampled at 2.5–5 kHz and filtered off-line at 1–5 kHz. The whole-cell ramp protocol consisted of a 500-ms ramp from −150 to +150 mV from a holding potential of 0 mV. The protocol used for the fractional Ca^{2+} current measurements consisted of a 10-s step to +80 mV, during which solution exchange was achieved, followed by a 1-s step to −80 mV and a 2-s step to +80 mV. Single-channel traces were sampled at 2 kHz and not filtered. The single-channel step protocol consisted of a 250-ms voltage step to −80 mV from a holding potential of 0 mV, followed by a 250-ms voltage step to voltages between +60 and +140 mV. The single-channel ramp protocol consisted of a 650-ms ramp from −100 to +100 mV from a holding potential of 0 mV.

During fractional Ca^{2+} current experiments, the cell was illuminated at 380 nm using a monochromator-based system (Polychrome IV, Till Photonics, Munich, Germany), and the Fura-2 fluorescence was detected using a photodiode. Illumination and fluorescence detection were controlled with Patchmaster software.

Measurement of intracellular Ca^{2+}

Cells were incubated with 2 μM Fura-2 acetoxymethyl ester for 30 min at 37°C. The fluorescent signal was measured during illumination alternating between 350 and 380 nm on a CellM fluorescence microscope (Olympus, Melville, NY). After correction for the individual background fluorescence signals, the ratio of the fluorescence values at the two excitation wavelengths (F_{350}/F_{380}) was determined. Absolute $[Ca^{2+}]_i$ values were calculated from fluorescence ratios using the Grynkiewicz equation (22), with parameters obtained during an in vivo calibration procedure.

Calculation of the relative permeability of mono- and divalent cations

The permeability of different monovalent cations relative to that of Na^+ (P_X/P_{Na}) was calculated from the reversal potential under biionic conditions according to

$$P_x/P_{\mathrm{Na}} = \exp\left(V_{\mathrm{rev}} \times F/RT\right), \tag{1}$$

where V_{rev} is the measured reversal potential after correction for liquid junction potentials, F is Faraday's constant, R is the universal gas constant, and T is the absolute temperature (23). Permeability of the divalent cations Ca^{2+} and Mg^{2+} relative to that of Na^+ was calculated from the absolute reversal potential measured with 100 mM of the respective cation in the extracellular solution, according to

$$P_x/P_{\mathrm{Na}} = \frac{\gamma_{\mathrm{Na}}[Na^+]_i}{4\gamma_X[X^{2+}]_o}\exp\left(V_{\mathrm{rev}}F/RT\right) \times \left(1 + \exp\left(V_{\mathrm{rev}}F/RT\right)\right), \tag{2}$$

where γ_{Na} and γ_X represent the activity coefficients for Na^+ and divalent cations, respectively (24). Activity coefficients were calculated according to the Debye-Hückel equation.

Quantification of FM1-43 uptake

To examine the cellular uptake of FM1-43, the fluorescence at 488 nm was monitored on an Olympus CellM fluorescence microscope at 5-s intervals. Cells were perfused with 10 μM FM1-43 for 90 s, and the sustained increase in fluorescence intensity was determined 90 s after washout of FM1-43. MO (20 μM) or ruthenium red (10 μM) was added to the extracellular solution, as described below.

Data analysis

Electrophysiological data were analyzed using the WinASCD software (G. Droogmans, Leuven, Belgium, http://www.kuleuven.be/fysio/trp/content/winascd-manual). Statistical analysis and graphical presentations were performed using the Origin version 7.0 software (OriginLab, Northampton, MA). Pooled data are given as the mean ± SE. Amplitude histograms were obtained from Gaussian multipeak fitting routines from Origin. Significance was tested using Student's paired t-test, and $P < 0.05$ was considered statistically significant. In the figures, significance is indicated by a single or double asterisk ($P < 0.05$ and $P < 0.01$, respectively).

RESULTS

Monovalent cation permeability and the TRPA1 pore diameter

We analyzed the permeability of TRPA1 to a set of inorganic and organic monovalent cations, to obtain information on the

field strength of the pore as well as on its diameter at the narrowest point. The permeability of different monovalent cations relative to that of Na^+ (P_X/P_{Na}) was determined by measuring the biionic reversal potential of the constitutive TRPA1 current after complete substitution of extracellular Na^+ by the specific cation. For inorganic monovalent cations, this analysis yielded (Fig. 1, *A* and *B*) $P_{Rb}/P_{Na} = 1.30 \pm 0.02$ ($n = 6$), $P_K/P_{Na} = 1.29 \pm 0.01$ ($n = 6$), $P_{Cs}/P_{Na} = 1.22 \pm 0.01$ ($n = 12$), and $P_{Li}/P_{Na} = 0.84 \pm 0.07$ ($n = 4$). The deduced monovalent cation permeability sequence ($Rb^+ \geq K^+ > Cs^+ > Na^+ > Li^+$) corresponds to Eisenman sequence III or IV, implying a weak field strength site.

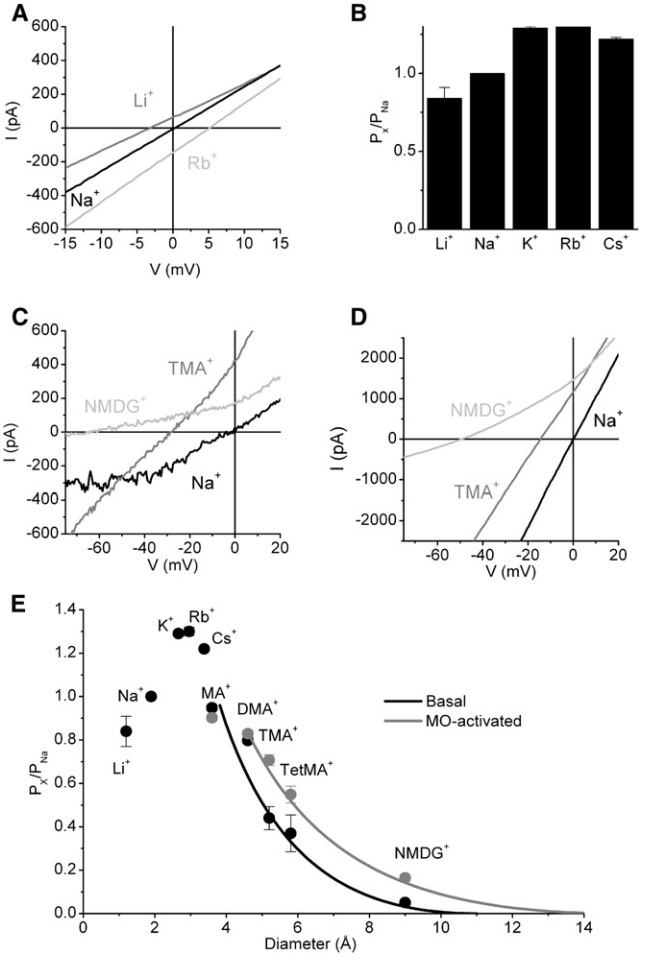

FIGURE 1 Monovalent cation permeability of TRPA1. (*A*) Current-voltage (IV) relations for anorganic monovalent cation currents through nonstimulated TRPA1 channels. The internal solution contained 150 mM Na^+ and the external solutions contained 150 mM of the indicated cation. (*B*) P_X/P_{Na} values for the different anorganic monovalent cations obtained from the reversal potential of experiments in *A*. (*C* and *D*) IV relations for external solutions containing 150 mM of Na^+ or the indicated organic cations obtained before (*C*) and during (*D*) stimulation with 20 μM MO. (*E*) Plot of the P_X/P_{Na} values for the different (an)organic cations versus their minimum diameters. For the organic cations, values were determined both before (*black*) and during (*red*) stimulation with 20 μM MO. Solid lines represent best fits to the data for the four largest cations, using Eq. 3, which yielded pore diameters of 11.0 and 13.8 Å before and during MO stimulation, respectively. Each data point represents the mean ± SE from at least five cells.

We next investigated the channel's ability to allow passage of organic cations with increasing diameter by measuring the relative permeability of monomethylammonium (MA^+; diameter (a) = 3.6 Å), dimethylammonium (DMA^+; a = 4.6 Å), trimethylammonium ($TriMA^+$; a = 5.2 Å), tetramethylammonium ($TetMA^+$; a = 5.8 Å), and N-methyl-D-glucamine ($NMDG^+$; a = 9 Å) compared to that of Na^+ (a = 1.9 Å; Fig. 1 *C*). Fig. 1 *E* plots the obtained permeability ratios of the different organic cations versus their estimated diameter. The data for the four largest cations were fitted using the excluded-volume equation (25)

$$\frac{P_X}{P_{Na}} = \frac{k\left(1 - a/d\right)^2}{a}, \tag{3}$$

which yielded an apparent pore diameter (d) of 11.0 Å.

It was recently shown that the relative permeability of TRPA1 to $NMDG^+$ increases upon agonist stimulation (26), suggesting agonist-dependent TRPA1 pore dilatation similar to what has been shown for the related TRPV1 channel. In line herewith, we found a significant increase of the relative permeability of TRPA1 to the larger cations, $TriMA^+$, $TetMA^+$, and $NMDG^+$, after stimulation with MO (Fig. 1, *D* and *E*). A fit of the data using the excluded-volume equation yielded an apparent pore diameter of 13.8 Å, suggesting that stimulation with MO leads to a dilatation at the narrowest point of the TRPA1 pore of ~3 Å.

To exclude the possibility that the MO-induced changes in biionic reversal potential for the large cations were due to activation of a TRPA1-independent leak conductance, we also performed some experiments using HC030031. This compound inhibits TRPA1 with a half-maximum inhibitory concentration value of ~1 μM and has little effect on other conductances (27), although some inhibitory effect on rat TRPV1 was recently reported (28). This approach allowed us to determine the reversal potential of the HC030031-sensitive current, which in CHO cells is exclusively mediated by TRPA1 channels. Using $NMDG^+$ as the sole extracellular cation, we found that reversal potential of the HC030031-sensitive current changed from -84 ± 6 mV before stimulation to -34 ± 8 mV during stimulation with MO (Fig. S1 in the Supporting Material). These data correspond to a change in P_{NMDG}/P_{Na} from 0.035 to 0.25, and thus fully endorse the results shown in Fig. 1. We conclude that the MO-induced changes in biionic reversal potential are due to genuine alterations of the pore properties of TRPA1, and that the contribution of TRPA1-independent leak conductance to the measured reversal potential is small.

As an independent assay to estimate the minimum pore diameter, we also tested whether TRPA1 can function as an entry pathway for FM1-43, a cationic dye (a = 10.5 Å)

that is known to permeate other nonselective cation channels, including TRPV1, $P2X_2$, and hair-cell mechanotransduction channels (29,30). To address this, we exposed naïve and TRPA1-expressing CHO cells to FM1-43 for 90 s and determined the amount of FM1-43 uptake by measuring the difference between the fluorescence intensity before application of the dye and 90 s after washout of the dye (Fig. 2, *A* and *B*) at 475 nm. These experiments were performed in Ca^{2+}-free medium to prevent the contribution of Ca^{2+}-dependent processes such as exo- and endocytosis to FM1-43 internalization. We found that FM1-43 uptake was significantly higher in TRPA1-expressing CHO cells compared to naïve CHO cells (Fig. 2 *C*), in line with the known basal activity of TRPA1 at room temperature (5,21). Inhibition of the TRPA1 pore with 10 μM ruthenium red reduced the level of FM1-43 uptake in TRPA1-expressing cells to that in naïve CHO cells (Fig. 2 *C*). FM1-43 uptake in TRPA1-expressing CHO cells, but not in naïve CHO cells, was further enhanced by application of the TRPA1 agonist MO (Fig. 2 *C*). These data indicate that FM1-43 can enter cells via the TRPA1 pore, indicating a pore diameter of >10.5 Å. It should be noted that these experiments do not allow a quantitative comparison of the actual rate of FM1-43 flux through the channel, because the data in Fig. 2 *C* provide a measure of the steady-state increase in cellular FM1-43 fluorescence, not the rate of fluorescence increase.

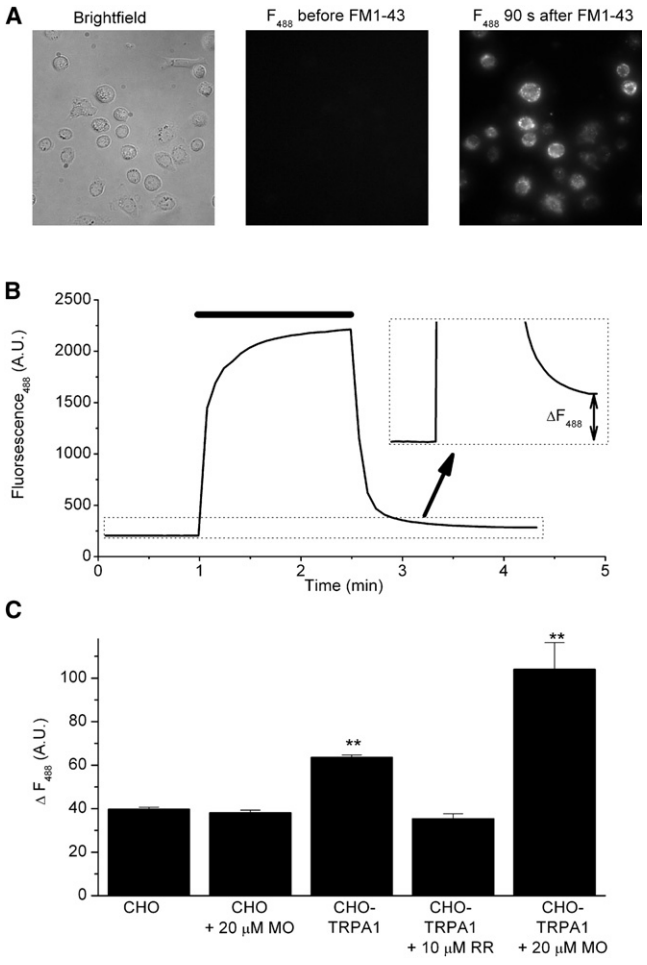

FIGURE 2 TRPA1-dependent uptake of FM1-43. (*A*) Representative brightfield image (*left*), and fluorescence images (excitation at 488 nm) before (*middle*) and after (*right*) incubation of TRPA1-expressing CHO cells with FM1-43 (10 μM). (*B*) Representative time course of the fluorescence signal at 488 nm (F_{488}). Cellular FM1-43 uptake was quantified as the persistent increase in F_{488} after full washout of FM1-43 (ΔF_{488}). (*C*) Comparison of FM1-43 uptake by naïve CHO cells, cells expressing TRPA1, and TRPA1-expressing cells treated with agonist (MO, 20 μM) or antagonist (ruthenium red, 10 μM), with 50–200 cells/condition.

We next investigated whether the MO-induced alterations in the TRPA1 pore also affect the channel's single-channel conductance. In cell-attached recordings, we found that application of MO caused a significant alteration of the single-channel current at +80 mV, which increased from 8.6 ± 0.2 pA before to 10.0 ± 0.5 pA during application of MO ($n = 5$, $P = 0.02$; Fig. 3, *A* and *B*). The single-channel conductance for outward currents at potentials between +60 and +140 mV increased from 113 to 134 pS (Fig. 3 *C*), whereas the inward single-channel conductance was not significantly altered (Fig. 3, *A–C*). A similar increase in outward conductance was observed in cell-attached patches (Fig. 3, *D* and *E*). We conclude that MO-induced changes in the TRPA1 pore also lead to small but significant alterations in the ion flux rate through individual open channels.

Divalent cation permeability and the fractional Ca^{2+} current

Previous works have revealed that TRPA1 is a Ca^{2+}-permeable, nonselective cation channel (reported P_{Ca}/P_{Na} values range from 0.84 to 3.28) (1,20), and that mutations at Asp^{918} in the putative pore region have a drastic effect on the channel's relative Ca^{2+} permeability (20). In addition, it has been reported that Mg^{2+} can permeate TRPA1, with a P_{Mg}/P_{Na} value of 1.23 (1). We were interested to investigate whether MO stimulation also influences the permeation of divalent cations through WT TRPA1 and TRPA1 mutated at Asp^{918}. It should be noted here that the estimated diameter of a Ca^{2+} ion ($a = 1.95$ Å) is almost identical to that of a Na^+ ion, whereas Mg^{2+} is clearly smaller ($a = 1.3$ Å). Thus, solely based on molecular sieving, an expansion of the pore is not expected to increase the relative permeability of these divalent cations. However, we considered that dynamic changes in the TRPA1 pore would alter the electrostatic properties of the conduction pathway, which may potentially affect the relative permeability of divalent versus monovalent cations.

To investigate this, we first compared P_{Ca}/P_{Na} and P_{Mg}/P_{Na} for WT TRPA1, both for nonstimulated channels and after channel stimulation with MO, by measuring the bionic reversal potential after complete substitution of extracellular Na^+ by 100 mM $CaCl_2$ (Fig. 4, *A*, *B*, and *E*) or

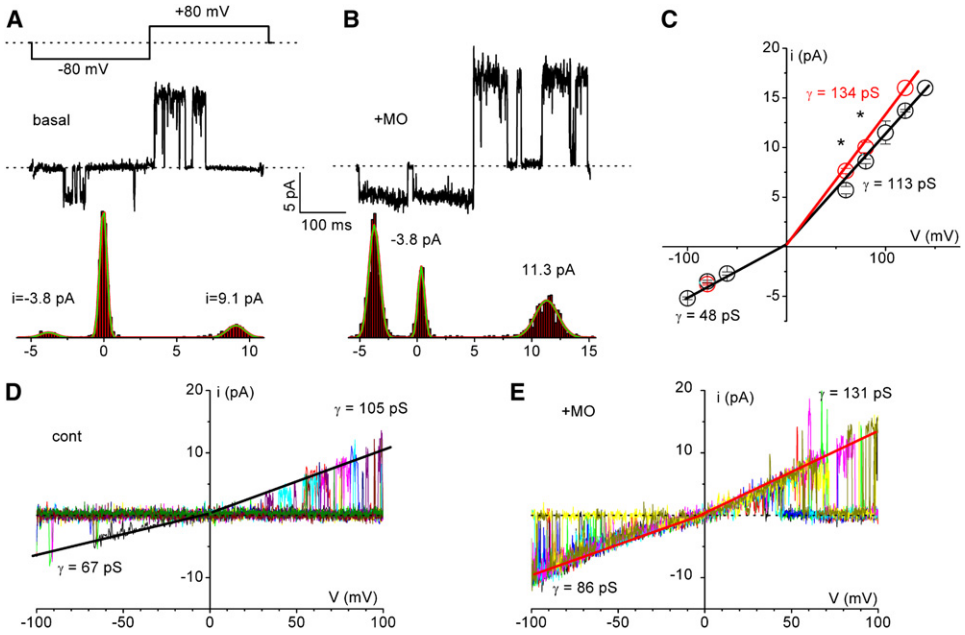

FIGURE 3 Stimulus-dependent changes in single-channel conductance. (*A* and *B*) Comparison between single-channel current traces in inside-out patches before (*A*) and during (*B*) stimulation with 20 μM MO. The pipette solution contained 5 mM $MgCl_2$. Current amplitudes were determined from the corresponding histograms (*lower*) by fitting of Gaussian functions. (*C*) Single-channel IV curves obtained before (*black*) and during (*red*) stimulation with MO. Lines represent linear fits forced through the origin. (*D* and *E*) Superimposed single-channel current traces obtained during voltage ramps in the cell-attached configuration before (*A*) and during (*B*) stimulation with 20 μM MO. The pipette solution contained 1 mM $MgCl_2$. A linear approximation of the inward and outward open-channel current level was fit by eye, yielding the indicated conductances. This experiment is representative of five similar cell-attached recordings.

$MgCl_2$ (Fig. 5, *A*, *B*, and *E*). Under basal conditions, this yielded values for P_{Ca}/P_{Na} and P_{Mg}/P_{Na} of 5.71 ± 0.38 and 1.72 ± 0.10, respectively (Figs. 4 *E* and 5 *E*). After determination of the basal Ca^{2+} and Mg^{2+} permeability ratios, cells were stimulated in divalent-cation-free solution with 20 μM MO for 3 min, and the bionic reversal potentials in 100 mM $CaCl_2$ or $MgCl_2$ were determined again (Figs. 4 *B* and 5 *B*). It should be noted that this analysis revealed a significant increase in relative permeability for both cations, with P_{Ca}/P_{Na} and P_{Mg}/P_{Na} values of 7.91 ± 0.60 and 3.75 ± 0.08, respectively (Figs. 4 *E* and 5 *E*). Note that these P_{Ca}/P_{Na} values are significantly higher than recently published values determined under comparable conditions by Wang et al. (20). We attribute this to the fact that those authors (20) based their calculations on ion concentrations, whereas we used ionic activity, as described in Eq. 2, which leads to P_{Ca}/P_{Na} values ~2.5-fold higher.

We then analyzed how mutations at Asp^{918} in the putative TRPA1 pore affect divalent cation permeability of TRPA1. In line with previous work, we found that different charge-neutralizing mutants (D918A, D918C, and D918Q) exhibited a significantly reduced relative Ca^{2+} permeability (20), with P_{Ca}/P_{Na} values of 0.47 ± 0.03, 1.06 ± 0.06, and 1.04 ± 0.08, respectively (Fig. 4, *C* and *E*). Likewise, the Mg^{2+} permeability of these three mutants was much lower than in WT TRPA1 (P_{Mg}/P_{Na} values of 0.27 ± 0.05, 0.73 ± 0.03, and 0.74 ± 0.12, respectively; Fig. 5, *C* and *E*). In contrast to WT TRPA1, MO stimulation of these pore mutants led to a decrease rather than an increase in relative Ca^{2+} or Mg^{2+} permeability (Figs. 4, *D* and *E*, and 5, *D* and *E*).

It should be noted that the above-described P_{Ca}/P_{Na} values quantify the relative permeability of Ca^{2+} versus Na^+ at the biionic reversal potential, and with a nonphysiological extracellular Ca^{2+} concentration (100 mM). They do not provide conclusive information on the Ca^{2+} flux through TRPA1 at membrane potentials and ionic conditions experienced by TRPA1-expressing cells such as sensory neurons or even transfected cell lines. When measuring the intracellular Ca^{2+} concentration ($[Ca^{2+}]_i$) in CHO cells bathed in a solution containing 2 mM Ca^{2+}, we observed significantly elevated $[Ca^{2+}]_i$ levels, not only in cells expressing WT TRPA1 but also, to a lesser extent, in cells expressing the D918A, D918C, and D918Q mutants, which indicates a significant basal Ca^{2+} influx (Fig. S2). Moreover, application of 2 mM Ca^{2+} after preactivating the channels with MO evoked a rapid rise in cells expressing WT TRPA1 and the different pore mutants, indicating robust MO-stimulated Ca^{2+} influx through these channels (Fig. S2). As expected from the P_{Ca}/P_{Na} values, stronger Ca^{2+} signals were observed in the cells expressing WT TRPA1 compared to those expressing pore mutants. However, these data do not allow a quantitative determination and comparison of the Ca^{2+} flux through the WT and mutant pores, because critical factors such as membrane potential and channel density were not controlled.

To address this point, we used combined patch-clamp and photometry measurements (31) to accurately estimate the fraction of the TRPA1-mediated current that is carried by Ca^{2+} (Pf%) at a membrane potential of −80 mV and with typical extracellular ionic concentrations of Ca^{2+} (2 mM), Mg^{2+} (1.5 mM), and Na^+ (150 mM). Cells expressing WT or mutant TRPA1 were kept in a Ca^{2+}-free medium and dialyzed for >5 min with a patch pipette containing a high concentration (2 mM) of the calcium-sensitive dye Fura-2. Because Fura-2 acts as a high-affinity Ca^{2+} chelator, this

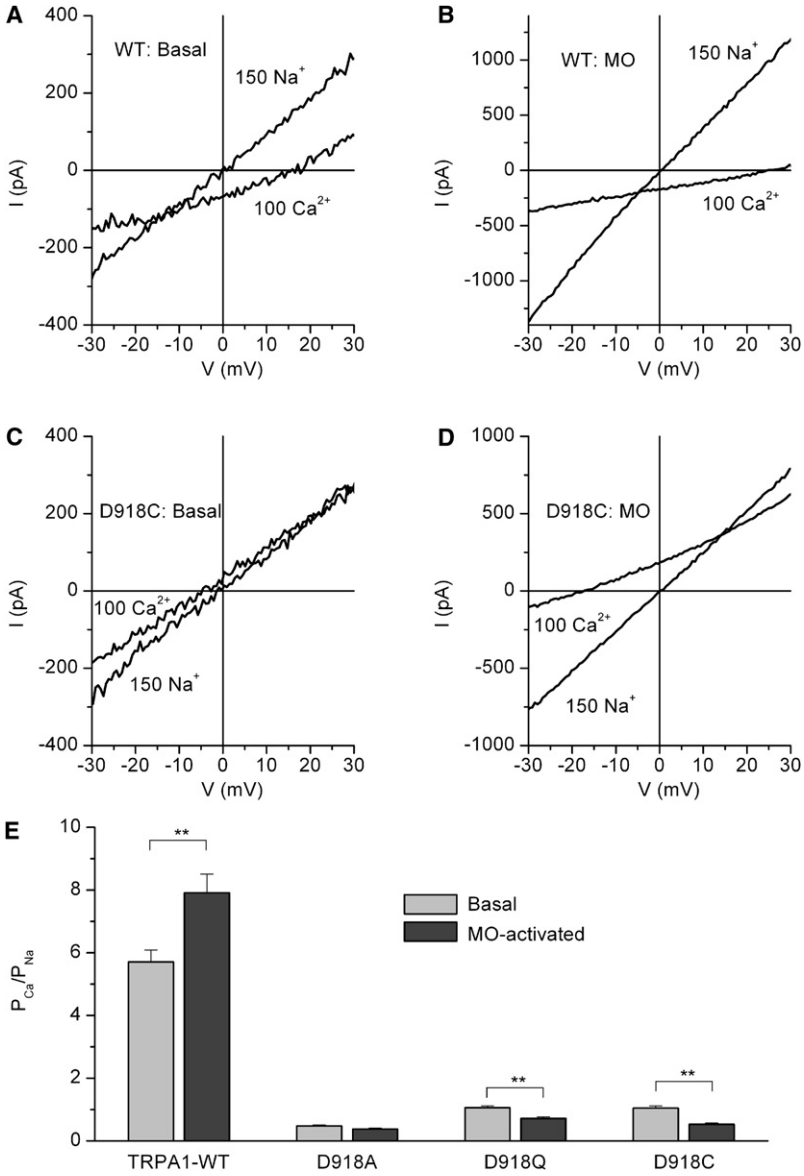

FIGURE 4 Stimulus-dependent changes in relative Ca^{2+} permeability. (*A* and *B*) Comparison of the IV relations obtained with external solutions containing 150 mM Na^+ or 100 mM Ca^{2+} as the sole extracellular cation, before (*A*) and during (*B*) stimulation with 20 μM MO. (*C* and *D*) Same as *A* and *B*, but for the TRPA1 pore mutant D918C. (*E*) P_{Ca}/P_{Na} values for WT TRPA1 and the different mutants obtained before and during stimulation with 20 μM MO. Each data point represents the mean ± SE from at least five cells.

ensures that the cytosolic Ca^{2+} level is strongly buffered at low nanomolar concentration (<20 nM). Moreover, in the dialyzed cells, Fura-2 is in strong excess over the endogenous Ca^{2+} buffers of the cell, such that virtually all Ca^{2+} ions entering the cytosol bind to Fura-2 (31). Hence, total Ca^{2+} influx is directly related to the decrease of Fura-2 fluorescence at 380 nM (F_{380}).

After full equilibration, the membrane potential was stepped to +80 mV and the extracellular medium was rapidly changed to a solution containing 2 mM Ca^{2+}. Then, a 1-s voltage step to −80 mV was imposed, causing an inward TRPA1 current and a concomitant decrease in F_{380} (Fig. 6 *A*). After this procedure, the cells were kept in Ca^{2+}-free solution to allow restoration of the low intracellular Ca^{2+} concentration and recovery of F_{380}. After a recovery period of 5 min, the voltage step procedure was repeated, but now using an extracellular solution containing isotonic $CaCl_2$ (100 mM; Fig. 6 *A*). Under this condition, the inward TRPA1 current is carried by Ca^{2+} ions exclusively, which allows determination of the relation between inward Ca^{2+} current and the decrease of F_{380} for each cell. Pf% was then determined as

$$Pf\% = 100 \times \frac{\int I_{100}dt}{\int I_2 dt} \times \frac{\Delta F_{380,2}}{\Delta F_{380,100}}, \qquad (4)$$

where I_2 and I_{100} represent the current during the 1-s voltage step to −80 mV in 2 and 100 mM Ca^{2+}, respectively, and $\Delta F_{380,2}$ and $\Delta F_{380,100}$ the corresponding decreases in Fura-2 fluorescence at 380 nM. For WT TRPA1, in the absence of agonist stimulation, this analysis yielded a Pf% of 17.0 ± 1.7% ($n = 5$). It should be noted that we obtained a significantly higher Pf% value of 23.3 ± 1.3% ($n = 5$) after

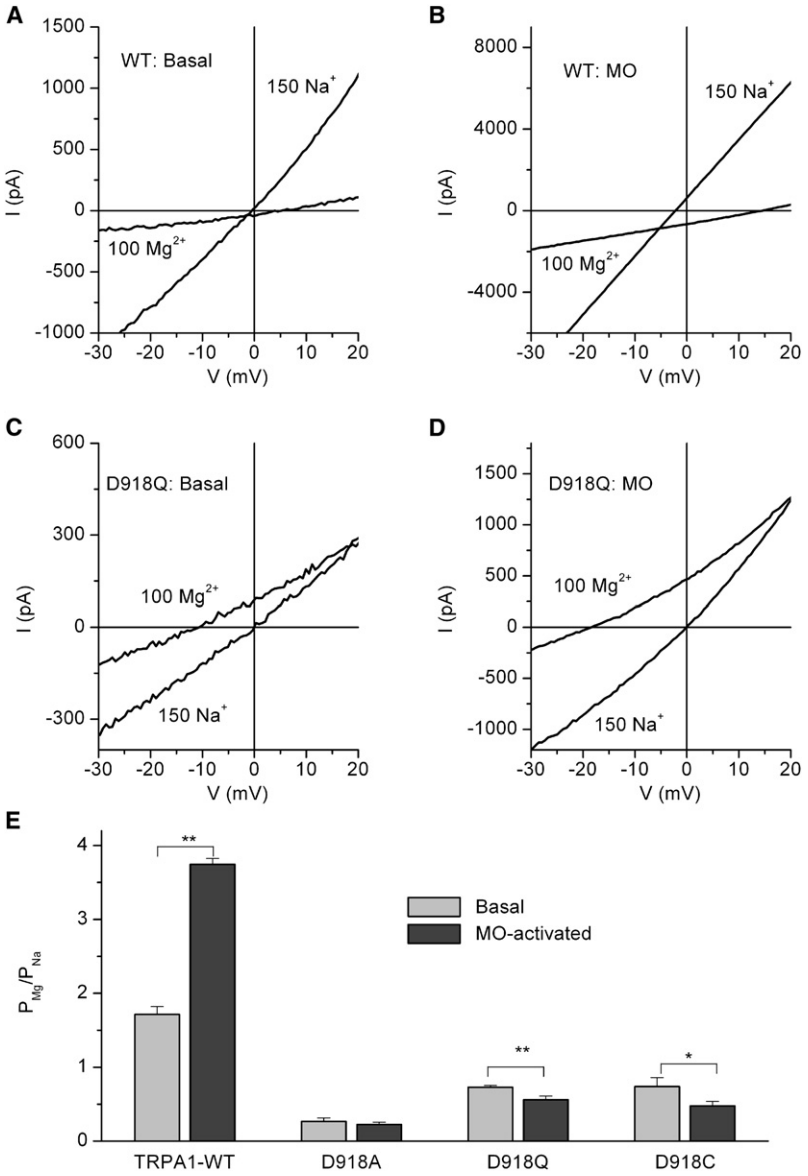

FIGURE 5 Stimulus-dependent changes in relative Mg^{2+} permeability. (*A* and *B*) Comparison of the IV relations obtained with external solutions containing 150 mM Na^+ or 100 mM Mg^{2+} as the sole extracellular cation, before (*A*) and during (*B*) stimulation with 20 μM MO. (*C* and *D*) Same as *A* and *B*, but for the TRPA1 pore mutant D918Q. (*E*) P_{Mg}/P_{Na} values for WT TRPA1 and the different mutants obtained before and during stimulation with 20 μM MO. Each data point represents the mean ± SE from at least five cells.

stimulation for 2 min with MO, in agreement with the reversal potential measurements (Fig. 6 *B*). These data indicate that even in physiological ionic conditions, a substantial fraction of the TRPA1 current is carried by Ca^{2+}, and that this fraction further increases upon MO stimulation. To exclude the possibility that these Pf% measurements are influenced by TRPA1-independent Ca^{2+} influx or leak current, we repeated these latter experiments in the presence of 20 μM of the TRPA1 antagonist HC030031. Under this condition, both ΔF_{380} and the integrated inward current were reduced by ~95% (Fig. S3), indicating that the influence of TRPA1-independent conductances on the Pf% estimates is small.

Similar experiments were performed in cells transfected with the three pore mutants. This yielded Pf% values significantly lower than those for WT TRPA1: 1.4 ± 0.4% for D918A, 4.6 ± 0.5% for D918C, and 5.3 ± 1.5% for D918Q (Fig. 6 *C*). Moreover, in contrast to WT TRPA1, MO stimulation did not cause a significant change in Pf% in these mutants (Fig. 6 *C*).

DISCUSSION

TRPA1 is a Ca^{2+}-permeable nonselective cation channel that acts as a sensor for noxious cold and a variety of chemicals in nociceptive neurons (1–3,5,27). Ca^{2+} not only acts as a permeant ion, but also controls activation and desensitization of TRPA1, resulting in a complex dependence of TRPA1 activity on extracellular Ca^{2+} (20,21). Until now, the actual Ca^{2+} flux through an open TRPA1 pore under physiological conditions was not known, nor was it understood how agonists influence the channel's permeability profile.

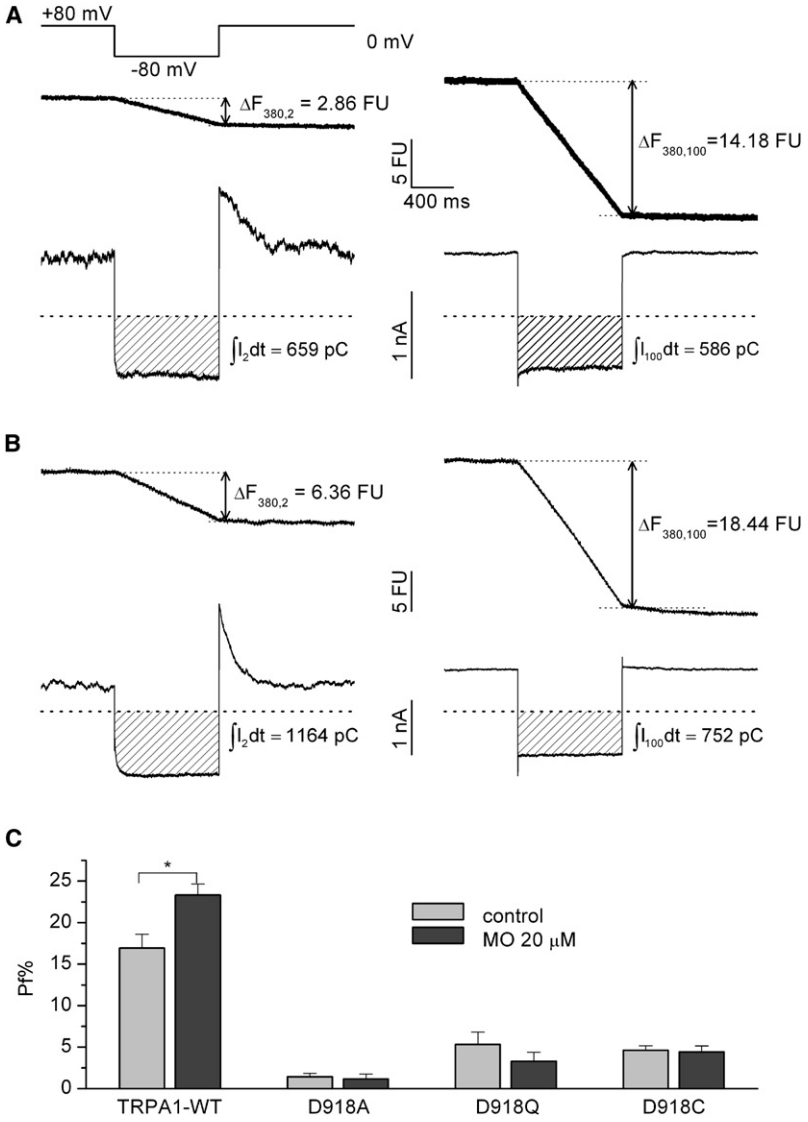

FIGURE 6 Fractional Ca^{2+} currents through TRPA1. (*A*) Representative example of the determination of Pf% for the nonstimulated WT TRPA1 current. The decrease in Fura2-fluorescence at 380 nm (in arbitrary fluorescence units (*FU*)) and the integrated inward current were measured during a 1-s step to −80 mV from a holding potential of +80 mV (protocol shown above), in extracellular solution containing 2 mM (*left*) or 100 mM (*right*) Ca^{2+}. Using Eq. 4, this recording yielded a Pf% of 17.9%. (*B*) Same as *A*, but in a cell stimulated with 20 μM MO. Using 4, this recording yielded a Pf% of 22.3%. (*C*) Average Pf% values for WT and mutant TRPA1, in both nonstimulated and MO-stimulated conditions. Each data point represents the mean ± SE from at least five cells.

The results presented in this article provide important novel information on the dimensions of the TRPA1 pore and the contribution of Ca^{2+} to the inward TRPA1 current. Furthermore, we present evidence that stimulation of TRPA1 with the strong agonist MO evokes both pore dilation and increased Ca^{2+} permeability and selectivity.

The most striking finding of our study is the large contribution of Ca^{2+} to the inward TRPA1 current under conditions that resemble those experienced by the channel in its native environment, i.e., with 2 mM extracellular Ca^{2+} ions and at a membrane potential of −80 mV. Using combined patch-clamp and Fura-2 fluorescence measurements, we measured a fractional Ca^{2+} current of 17% for basal TRPA1 activity and up to 23% after stimulation with MO. Assuming the validity of the Goldman-Hodgkin-Katz (GHK) equation for ionic currents, which implies independent movement of ions in the pore (32), Pf% values can be directly calculated from P_{Ca}/P_{Na} values according to the equation

$$Pf\% = 100 \times \frac{4\gamma_{Ca}[Ca^{2+}]_o}{4\gamma_{Ca}[Ca^{2+}]_o + \frac{P_{Na}}{P_{Ca}}\gamma_{Na}[Na^+]\left(1 - e^{\frac{2FV_m}{RT}}\right)}, \quad (5)$$

where $[Na^+]$ represents the symmetrical Na^+ concentration present in the intra- and extracellular solutions (150 mM in our Pf% experiments; see Frings et al. (33)). In Fig. 6, experimental Pf% values for WT and mutant TRPA1, both before and after MO stimulation, are plotted versus the corresponding P_{Ca}/P_{Na} values obtained from biionic reversal potentials, and compared with the predictions of the GHK equation. It should be noted that Pf% values for WT TRPA1 and mutants D918C and D918Q are significantly higher than would be predicted from reversal potential measurements. In contrast, Pf% values for the Ca^{2+} currents through acid- or capsaicin-activated TRPV1 (24,34) are significantly lower than would be expected from P_{Ca}/P_{Na} measurements (Fig. 7). Thus,

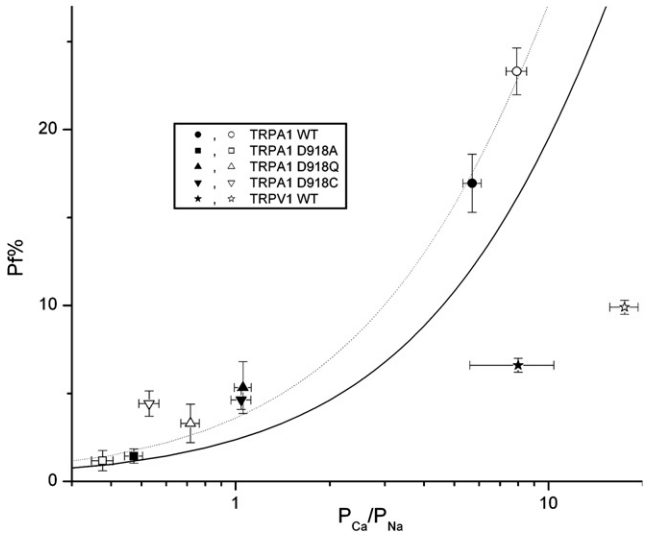

FIGURE 7 Comparison of P_{Ca}/P_{Na} and Pf% values for WT and mutant TRPA1 and for TRPV1. For TRPA1, solid symbols represent the basal state and open symbols the MO-activated state. For TRPV1, the solid and open symbols represent the current activated by pH 5 and 100 nM capsaicin, respectively (values taken from Chung et al. (24) and Samways et al. (34)). Solid line represents the prediction of the GHK-equation (Eq. 5). The dotted line represents a modified GHK equation assuming that Ca^{2+} ions provoke 35% block of the monovalent cation current.

despite the fact that the relative Ca^{2+} permeability (P_{Ca}/P_{Na}) of TRPV1 under different stimulation conditions is two- to fourfold higher than that of TRPA1, the latter channel seems better able to allow inward Ca^{2+} fluxes under physiological conditions. This implies that for a similar level of channel activity, TRPA1 will evoke a larger Ca^{2+} signal than TRPV1, which may have important consequences for the Ca^{2+}-dependent processes that occur in nociceptor neurons, including the release of neuropeptides and regulation of the activation and inactivation of TRPV1 and TRPA1. The high Pf% of TRPA1 may also help to explain why TRPA1-overexpressing cells are generally overloaded with Ca^{2+}, as evidenced by average cytosolic Ca^{2+} levels of ~1 μM (see, e.g., Fig. S1).

What could be the mechanism underlying the high fractional Ca^{2+} current through the TRPA1 pore? In highly Ca^{2+}-selective pores, such as those of TRPV5/6, Ca_V, and calcium-release-activated calcium channels, selectivity for Ca^{2+} over Na^+ is thought to arise from the binding of Ca^{2+} to one or more high-affinity sites in the lumen of the pore (23,32). In the absence of Ca^{2+}, these channels carry large monovalent cation currents, but low micromolar concentrations of Ca^{2+} (or other divalents) are generally sufficient to fully prevent the monovalent current. Although such a micromolar affinity block of monovalent cation flow does not occur in TRPA1, there are indications that millimolar concentrations of Ca^{2+} or other divalent cations can hinder monovalent cation currents. As indicated by the dotted line in Fig. 6, the Pf% values for WT TRPA1 can be reproduced assuming that Ca^{2+} induces a partial block (~35%) of the monovalent cation current, in line with published single-channel measurements (21).

In line with previous work, we found that charge-neutralizing mutations at Asp^{918} in the putative pore region of TRPA1 strongly reduce P_{Ca}/P_{Na} and P_{Mg}/P_{Na} values, suggesting that this residue is a critical determinant of the channel's Ca^{2+} selectivity (20). Yet, intracellular Ca^{2+} recordings revealed that these channels still mediate substantial Ca^{2+} influx under basal and MO-stimulated conditions, and Pf% values determined for these mutants ranged from 1.4% for D918A to 5.3% for D918C. Although these values are significantly lower than those for WT TRPA1, they fall within the range of values obtained for other Ca^{2+}-permeable nonselective cation channels, such as TRPV1 or the ionotropic receptors for glutamate or acetylcholine (34–36). At first glance, it may seem surprising that MO stimulation caused a small decrease, rather than an increase, of the Ca^{2+} permeability of mutants D918A and D918C. It should be noted, however, that Ca^{2+} and Na^+ ions have virtually the same dimensions, and that their relative permeability thus is determined by factors other than the diameter of the selectivity filter at its narrowest point, in particular, the distribution of charges in the permeation pathway. In the mutants where the dominant Asp^{918} is neutralized, the relative Ca^{2+} permeability will depend on the distribution of other, less dominant charges in the pore. Apparently, the MO-induced changes in the TRPA1 pore alter the distribution of these charges in such a way that Ca^{2+} permeability is slightly decreased.

Our analysis of the relative permeability of large organic cations and the cellular uptake of FM1-43 yielded an estimated TRPA1 pore diameter of at least 11.0 Å under basal conditions. This large pore diameter is comparable to estimates obtained for other Ca^{2+}-permeable nonselective TRP channels including TRPV1 (10.1 Å) (24), TRPM6 (11.5 Å) (37), and TRPP2 ($\geq$11 Å) (38), but is significantly larger than estimates for the highly Ca^{2+}-selective TRPV5 (7.5 Å at pH 7.4) (39) and TRPV6 (5.4 Å) (25). We note that the relative permeability of large organic cations increased significantly upon stimulation with the agonist MO, indicative of dilatation of the TRPA1 pore by at least 2 Å. In line herewith, we also found that MO alters the single-channel conductance of TRPA1. Our results are in agreement with those of a recent study showing agonist-induced increases in the permeability of TRPA1 for $NMDG^+$ (26). Note that the study by Chen et al. (26) did not address the actual dimension changes, the alterations at the single-channel level, or the changes in divalent cation permeability and fractional Ca^{2+} current. Agonist-dependent pore dilation has also been reported for TRPV1 (with capsaicin) (24) and TRPV5 (upon alkalinization) (39). In the case of TRPV5, evidence has been presented that pH-dependent changes in pore diameter reflect a rotation of the pore helix.

Further research is needed to investigate whether a similar mechanism modulates the pore diameter and divalent permeability of TRPA1.

In conclusion, we have shown that TRPA1 has a wide pore that allows a much larger flux of Ca^{2+} ions than would be predicted from previous reversal potential measurements. Moreover, our results provide evidence for a stimulus-dependent regulation of the Ca^{2+} permeability and diameter of the TRPA1 pore. Due to the high and stimulus-dependent Ca^{2+} flux through its pore, TRPA1 may represent an important determinant of the Ca^{2+} signal in nociceptors, thereby regulating various Ca^{2+}-dependent processes, including TRPA1 activation and inactivation, TRPV1 desensitization, and the release of neurotransmitters and inflammatory mediators.

SUPPORTING MATERIAL

Three figures are available at http://www.biophysj.org/biophysj/supplemental/S0006-3495(09)01731-7.

We thank M. Benoit for technical assistance and the members of our laboratory for helpful discussions. K.T. is a postdoctoral fellow of the Research Foundation-Flanders.

This work was supported by grants from the Belgian Ministry for Science Policy (Interuniversity Attraction Pole IUAP P6/28), the Research Foundation-Flanders (G.0172.03 and G.0565.07), and the Research Council of the Katholieke Universiteit Leuven (GOA 2004/07and EF/95/010).

REFERENCES

1. Story, G. M., A. M. Peier, …, A. Patapoutian. 2003. ANKTM1, a TRP-like channel expressed in nociceptive neurons, is activated by cold temperatures. *Cell.* 112:819–829.
2. Bautista, D. M., S. E. Jordt, …, D. Julius. 2006. TRPA1 mediates the inflammatory actions of environmental irritants and proalgesic agents. *Cell.* 124:1269–1282.
3. Kwan, K. Y., A. J. Allchorne, …, D. P. Corey. 2006. TRPA1 contributes to cold, mechanical, and chemical nociception but is not essential for hair-cell transduction. *Neuron.* 50:277–289.
4. García-Añoveros, J., and K. Nagata. 2007. TRPA1. *Handb. Exp. Pharmacol.* 179:347–362.
5. Karashima, Y., K. Talavera, …, T. Voets. 2009. TRPA1 acts as a cold sensor in vitro and in vivo. *Proc. Natl. Acad. Sci. USA.* 106: 1273–1278.
6. Doerner, J. F., G. Gisselmann, …, C. H. Wetzel. 2007. Transient receptor potential channel A1 is directly gated by calcium ions. *J. Biol. Chem.* 282:13180–13189.
7. Zurborg, S., B. Yurgionas, …, P. A. Heppenstall. 2007. Direct activation of the ion channel TRPA1 by Ca^{2+}. *Nat. Neurosci.* 10: 277–279.
8. Hu, H., M. Bandell, …, A. Patapoutian. 2009. Zinc activates damage-sensing TRPA1 ion channels. *Nat. Chem. Biol.* 5:183–190.
9. Fujita, F., K. Uchida, …, M. Tominaga. 2008. Intracellular alkalization causes pain sensation through activation of TRPA1 in mice. *J. Clin. Invest.* 118:4049–4057.
10. Bandell, M., G. M. Story, …, A. Patapoutian. 2004. Noxious cold ion channel TRPA1 is activated by pungent compounds and bradykinin. *Neuron.* 41:849–857.
11. Jordt, S. E., D. M. Bautista, …, D. Julius. 2004. Mustard oils and cannabinoids excite sensory nerve fibres through the TRP channel ANKTM1. *Nature.* 427:260–265.
12. Bang, S., and S. W. Hwang. 2009. Polymodal ligand sensitivity of TRPA1 and its modes of interactions. *J. Gen. Physiol.* 133:257–262.
13. Hinman, A., H. H. Chuang, …, D. Julius. 2006. TRP channel activation by reversible covalent modification. *Proc. Natl. Acad. Sci. USA.* 103:19564–19568.
14. Macpherson, L. J., A. E. Dubin, …, A. Patapoutian. 2007. Noxious compounds activate TRPA1 ion channels through covalent modification of cysteines. *Nature.* 445:541–545.
15. Karashima, Y., N. Damann, …, B. Nilius. 2007. Bimodal action of menthol on the transient receptor potential channel TRPA1. *J. Neurosci.* 27:9874–9884.
16. Fajardo, O., V. Meseguer, …, F. Viana. 2008. TRPA1 channels: novel targets of 1,4-dihydropyridines. *Channels (Austin).* 2:429–438.
17. Matta, J. A., P. M. Cornett, …, G. P. Ahern. 2008. General anesthetics activate a nociceptive ion channel to enhance pain and inflammation. *Proc. Natl. Acad. Sci. USA.* 105:8784–8789.
18. Xiao, B., A. E. Dubin, …, A. Patapoutian. 2008. Identification of transmembrane domain 5 as a critical molecular determinant of menthol sensitivity in mammalian TRPA1 channels. *J. Neurosci.* 28: 9640–9651.
19. Talavera, K., M. Gees, …, T. Voets. 2009. Nicotine activates the chemosensory cation channel TRPA1. *Nat. Neurosci.* 12:1293–1299.
20. Wang, Y. Y., R. B. Chang, …, E. R. Liman. 2008. The nociceptor ion channel TRPA1 is potentiated and inactivated by permeating calcium ions. *J. Biol. Chem.* 283:32691–32703.
21. Nagata, K., A. Duggan, …, J. García-Añoveros. 2005. Nociceptor and hair cell transducer properties of TRPA1, a channel for pain and hearing. *J. Neurosci.* 25:4052–4061.
22. Grynkiewicz, G., M. Poenie, and R. Y. Tsien. 1985. A new generation of Ca^{2+} indicators with greatly improved fluorescence properties. *J. Biol. Chem.* 260:3440–3450.
23. Owsianik, G., K. Talavera, …, B. Nilius. 2006. Permeation and selectivity of TRP channels. *Annu. Rev. Physiol.* 68:685–717.
24. Chung, M. K., A. D. Güler, and M. J. Caterina. 2008. TRPV1 shows dynamic ionic selectivity during agonist stimulation. *Nat. Neurosci.* 11:555–564.
25. Voets, T., A. Janssens, …, B. Nilius. 2004. Outer pore architecture of a Ca^{2+}-selective TRP channel. *J. Biol. Chem.* 279:15223–15230.
26. Chen, J., D. Kim, …, R. M. Reilly. 2009. Pore dilation occurs in TRPA1 but not in TRPM8 channels. *Mol. Pain.* 5:3.
27. McNamara, C. R., J. Mandel-Brehm, …, C. M. Fanger. 2007. TRPA1 mediates formalin-induced pain. *Proc. Natl. Acad. Sci. USA.* 104:13525–13530.
28. Iwasaki, Y., M. Tanabe, …, T. Watanabe. 2009. Miogadial and miogatrial with α,β-unsaturated 1,4-dialdehyde moieties—novel and potent TRPA1 agonists. *Life Sci.* 85:60–69.
29. Gale, J. E., W. Marcotti, …, G. P. Richardson. 2001. FM1-43 dye behaves as a permeant blocker of the hair-cell mechanotransducer channel. *J. Neurosci.* 21:7013–7025.
30. Meyers, J. R., R. B. MacDonald, …, D. P. Corey. 2003. Lighting up the senses: FM1-43 loading of sensory cells through nonselective ion channels. *J. Neurosci.* 23:4054–4065.
31. Neher, E. 1995. The use of fura-2 for estimating Ca buffers and Ca fluxes. *Neuropharmacology.* 34:1423–1442.
32. Hille, B. 2001. Ion Channels of Excitable Membrane, 3rd ed. Sinauer Associates, Sunderland, MA.
33. Frings, S., R. Seifert, …, U. B. Kaupp. 1995. Profoundly different calcium permeation and blockage determine the specific function of distinct cyclic nucleotide-gated channels. *Neuron.* 15:169–179.

34. Samways, D. S., B. S. Khakh, and T. M. Egan. 2008. Tunable calcium current through TRPV1 receptor channels. *J. Biol. Chem.* 283:31274–31278.

35. Burnashev, N., Z. Zhou, …, B. Sakmann. 1995. Fractional calcium currents through recombinant GluR channels of the NMDA, AMPA and kainate receptor subtypes. *J. Physiol.* 485:403–418.

36. Schneggenburger, R., Z. Zhou, …, E. Neher. 1993. Fractional contribution of calcium to the cation current through glutamate receptor channels. *Neuron.* 11:133–143.

37. Topala, C. N., W. T. Groenestege, …, R. J. Bindels. 2007. Molecular determinants of permeation through the cation channel TRPM6. *Cell Calcium.* 41:513–523.

38. Anyatonwu, G. I., and B. E. Ehrlich. 2005. Organic cation permeation through the channel formed by polycystin-2. *J. Biol. Chem.* 280:29488–29493.

39. Yeh, B. I., Y. K. Kim, …, C. L. Huang. 2005. Conformational changes of pore helix coupled to gating of TRPV5 by protons. *EMBO J.* 24:3224–3234.